COMPDYN 2013
4th ECCOMAS Thematic Conference on
Computational Methods in Structural Dynamics and Earthquake Engineering
M. Papadrakakis, V. Papadopoulos, V. Plevris (eds.)
Kos Island, Greece, 12–14 June 2013

CHARACTERISATION OF THE AERODYNAMIC BEHAVIOUR OF THE BRAGA STADIUM SUSPENSION ROOF FROM PROTOTYPE MONITORING

Elsa Caetano[1], Nuno Martins[1] and Álvaro Cunha[1]

[1] ViBest, Faculty of Engineering, University of Porto
R. Dr. Roberto Frias, 4200-465 Porto, Portugal
e-mail: ecaetano@fe.up.pt

Keywords: Suspension roof, Dynamic monitoring, Wind monitoring, Wind, Temperature, Modal variability.

Abstract. *The Laboratory of Vibrations and Structural Monitoring (ViBest) of the Faculty of Engineering of the University of Porto has installed dynamic and wind monitoring systems at the Braga Stadium suspension roof, including two sonic anemometers and various accelerometers operating continuously since 2009, aiming at providing a characterisation of the wind loads on the roof and establishing correlations with the response. This paper presents the most relevant properties of the wind measured on the prototype, establishing correlations with the measured accelerations, in order to validate numerical design studies, and analyses the influence of wind and temperature on the natural frequencies and modal damping ratios.*

1 INTRODUCTION

Designed by Eduardo Souto Moura in conjunction with Afassociados, the Braga Municipal Stadium was built for the 2004 European Football Championship that took place in Portugal [1].

A particular aspect of this structure is the suspension roof structure, formed by 34 pairs of cables spanning 202 m and supporting two composite slabs 0.245 m thick over the stands, in extensions of 57 m from the anchorages.

This very slender structure was object of various design studies, which comprehended numerical studies for dynamic assessment and wind tunnel tests on rigid and flexible physical models, to determine pressure coefficients, identify potential aeroelastic instabilities and assess the response to turbulent wind. These studies pointed in general to a risk of high vibrations due to resonant effects and of high local vortex shedding stresses.

These factors motivated extensive tests conducted on the constructed structure to assess damping, and the installation of a monitoring system in order to monitor the roof response under wind excitation.

In the context of the research activity of the Laboratory of Vibrations and Structural Monitoring (ViBest) of the Faculty of Engineering of the University of Porto, a complementary monitoring system was installed, including two sonic anemometers and various accelerometers, aiming at providing a characterisation of the wind loads on the roof and establishing correlations with the response.

The present paper aims at presenting the most relevant properties of the wind measured on prototype, establishing correlations with the measured accelerations, in order to validate numerical design studies, and analyses the influence of wind and temperature on the natural frequencies and modal damping ratios**.**

2 DESCRIPTION OF BRAGA STADIUM SUSPENSION ROOF

The present study is focused on the roof structure of the Braga Municipal Stadium, located in Braga, in the north west of Portugal (Figure 1). This infrastructure was built for the 2004 European Football Championship that took place in Portugal.

(a) (b)

Figure 1: (a) Top view and (b) perspective of the Braga Municipal Sports Stadium.

The stadium was constructed on the mountainside of Monte Castro, where one of the tribunes was built into the hill itself, and the second was erected on the other side of the pitch. While the north-west side of the stadium is wide open to the valley, a great granite massif stretches along the south-east side (Figures 1 and 2).

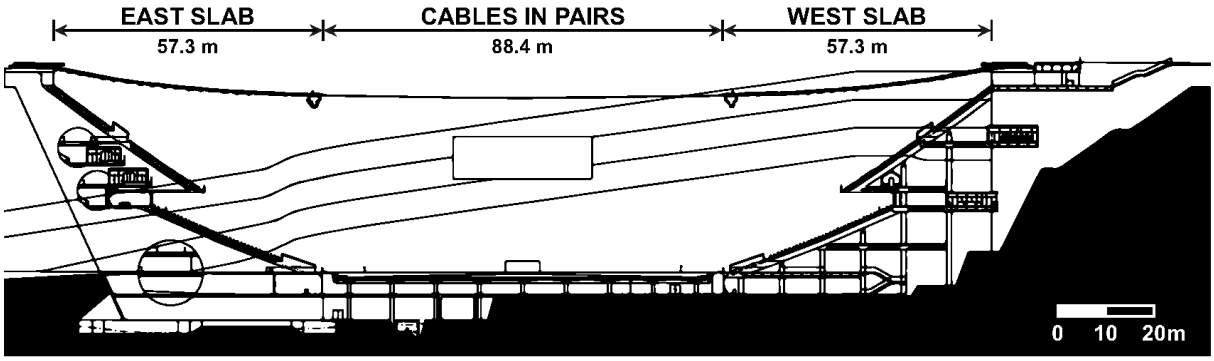

Figure 2: Longitudinal section of the stadium suspension roof.

The highlight of the stadium is its suspension roof shown also in Figures 1 and 2. The roof is composed by 34 pairs of full locked coil cables with diameters varying between 80 and 86 mm, spaced 3.75 m apart from each other. The cables span 202 m between the tops of both tribunes, supporting the two slabs on the first 57.3 m in each end, the central 88.4 m being free. The slender concrete slabs, only 0.245 m thick, are supported by the cables only in their normal direction, allowing for relative tangential movements between the two types of elements. A slight slope towards the south east side is achieved by a variation of the cables length, which allows the efficient drainage of the rainwater. A transversal triangular truss is suspended from the inner border of each slab acting as a stiffness beam and simultaneously accommodating the floodlights and loudspeakers. The roof cables are anchored in two large beams at the top of both tribunes – east and west. The east tribune (seen on the left in Figure 1(b) and in Figure 2) is structurally formed by 50 m high concrete walls, whose geometry was defined in order to minimise, at the level of the foundation, the unbalanced moments motivated by the combination of the gravitational action of the tribune and the high forces transmitted by the roof cables. In the west stand (seen on the right in Figure 1(b) and Figure 2), the concrete walls are anchored in the rock and the roof cable forces are transmitted to the foundation by prestressing tendons embedded in the concrete. The particular characteristics of the structure and the expected proneness to dynamic effects induced by the wind have motivated extensive studies developed during the design phase by various independent entities, with the purpose of adequately defining design loads and evaluating the corresponding static and dynamic behaviour [2-5]. The results provided by such studies as well as those obtained from numerical simulations and wind tunnel tests have demonstrated that the structure could be vulnerable to aeroelastic instabilities [5].

3 CONTINUOUS MONITORING OF THE ROOF STRUCTURE

The need of a strict control of the influence of environmental factors on the structural behaviour and geometry led to the installation of a static, dynamic and wind monitoring system during the construction of the structure [1]. The static monitoring system was essential during the construction and is based on a series of load cells installed in the cable anchorages, on embedded instrumentation of the concrete structure (strain gauges, tiltmeters and thermometers) and on instrumentation of the rock massifs and foundations with load cells installed in the anchors to the earth and in-place inclinometers. The dynamic monitoring system is important to observe the response of the roof to the wind excitation and is composed by 6 accelerometers, installed in the inner edges of the concrete slabs, and by cells to measure the wind pressure at various points on the underside and top of the roof slabs.

With the purpose of investigating the sensitivity of the structure to ambient effects and wind, ViBest/FEUP has installed two complementary monitoring systems on the west con-

crete slab: one to measure the dynamic response [6] and other to collect wind and temperature data [7]. The dynamic monitoring system has been active since March 2009 and has allowed the characterisation of the amplitudes of vibration of the slab, as well as the permanent identification of natural frequencies, modal shapes and modal damping ratios. The wind monitoring system was installed in December 2011, and is composed by two three-dimensional ultrasonic anemometers, suitable to measure wind velocities and directions, as well as sonic temperatures, at high sampling frequencies. The synchronisation of both measuring systems is enabled by accurate internal clocks set by GPS.

The installation of the two monitoring systems followed the layout represented in Figure 3 [7].

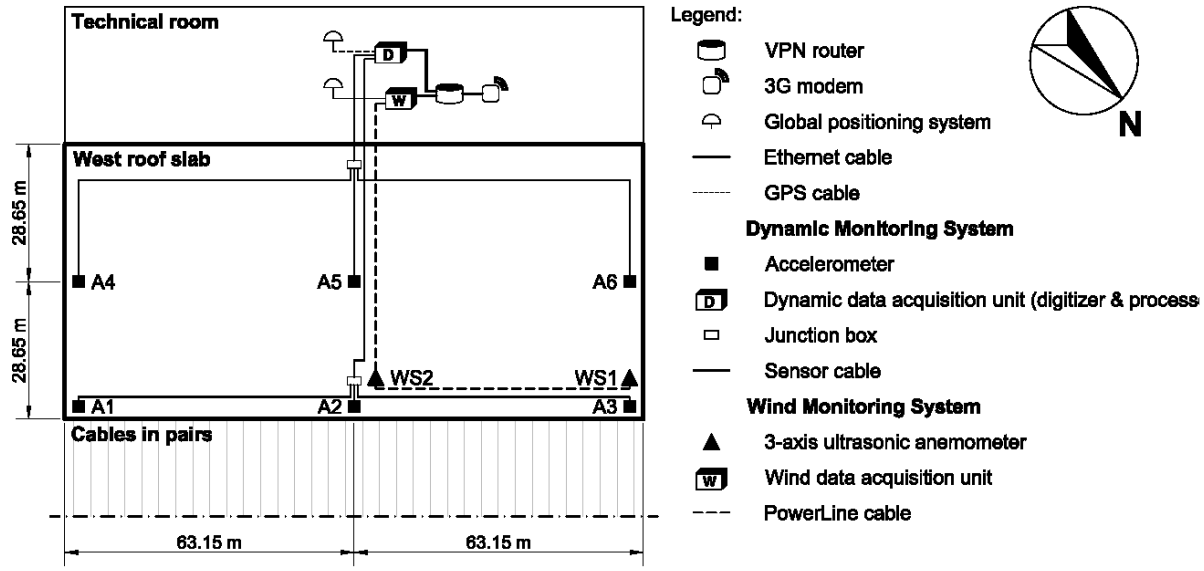

Figure 3: Partial plan of the Braga stadium roof (west roof slab) showing the location of the two monitoring systems installed for wind measurements and acquisition of vertical accelerations.

3.1 Dynamic monitoring system

The dynamic monitoring system is essentially composed by six force balance accelerometers, a digitizer and a robust field processor. The six accelerometers are distributed on the top of the west slab according to the scheme shown in Figure 3. The spatial distribution was defined with the goal of reasonably characterising at least the 10 first mode shapes identified in previous experimental and numerical works [8]. Two junction boxes group the signals of three sensors each in a single cable that is then linked to the acquisition system. The acquired acceleration records are then transmitted to the field processor through an Ethernet cable.

The field processor organises the acceleration time series sampled at 20 Hz in consecutive text files with a time duration of 60 minutes. The selection of this length for the time records resulted from a compromise between the goals of obtaining reliable estimates of modal damping ratios and a characterisation of the daily variations of the model parameters [6].

3.2 Wind measurement system

This system comprehends two three-dimensional ultrasonic anemometers which allow the characterisation of the wind through time averaged statistics of speed, direction and incidence angles, spectra and co-spectra of velocity components and temperature. These quantities can be subsequently used to assess the influence of the wind loading on the dynamic behaviour of the roof structure. According to the scheme and picture presented in Figure 3, the two ane-

mometers were placed on the top of the west slab, both along its inner edge, WS1 in the northernmost point, and WS2 in the middle of the slab [7], just next to accelerometers A3 and A2 from the dynamic monitoring system, respectively. Both sensors are mounted on masts 3 m high in order to reduce the interferences from the structure with the flow. A sampling rate of 10 Hz was chosen in order to efficiently measure the turbulent component of the wind flow [9]. The collected wind time series are then stored in text files with a length of 10 minutes.

4 FIELD MEASUREMENT OF WIND PARAMETERS

The three-dimensional ultrasonic anemometers were configured to record the wind speed as three wind speed components, each along one of the sonic orthogonal axes *x*, *y* or *z*. A coordinate rotation must be applied in order to obtain the mean wind speed, direction and elevation angles, as well as the turbulent component time series for the longitudinal, lateral and vertical directions. In this study, a double coordinate rotation scheme was used, described in some detail in [9, 10]. According to this approach, the streamline referential is redefined every block-averaging period. The block time series are averaged, from which results a mean wind speed vector defined in the sonic coordinate system *x*, *y*, *z* with sonic components ($\overline{u}_m$, $\overline{v}_m$, $\overline{w}_m$). The objective of the double rotation method is to impose $\overline{v} = \overline{w} = 0$, so that the total velocity vector is expressed by a streamline mean speed plus three orthogonal turbulent speed components (($\bar{U} + u'$), v', w'), a mean direction angle (γ) and a mean elevation angle (β).

The data presented herein corresponds to approximately eight months of continuous measurements, between mid-December 2011 and the first days of August 2012.

4.1 Mean wind speed, direction and elevation angles

Figure 4 shows the variation of the 10-min mean wind speed measured by the two sonic anemometers since the installation of the wind measurement system. From this representation, one can verify that the evolution of the mean wind speed is generally coherent through the entire time between the two instruments, the values measured by WS1 being commonly higher. The observed mean wind speed shows maximum values of 9.37 m/s and 7.22 m/s for ultrasonic anemometers WS1 and WS2, respectively. Nevertheless, it is possible to conclude that the mean wind speed measured is generally low, with most of the measurements below 4 m/s. Henceforward just the data points with a significant wind speed will be considered and all measurements with 10-min mean wind speed below 4 m/s will be discarded.

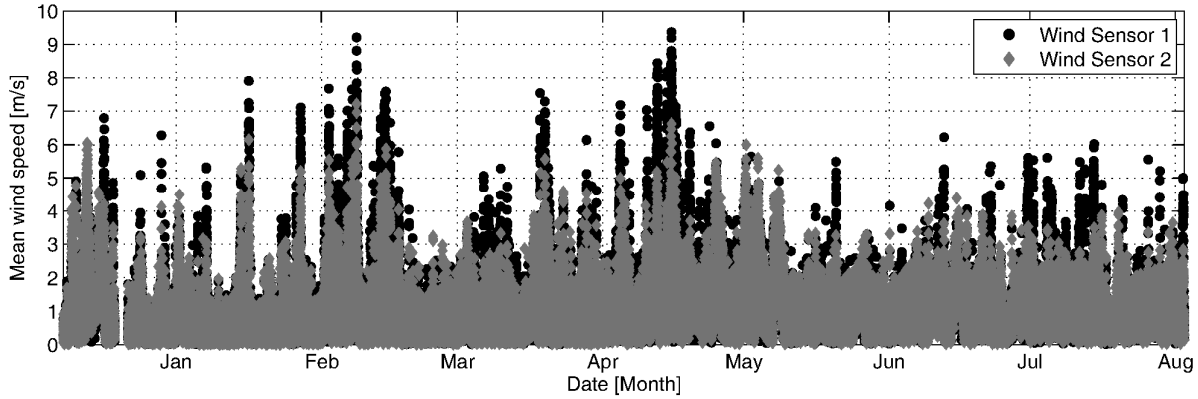

Figure 4: Time-history of 10-min mean wind speed measured by the two sonic anemometers over the period of 8 months.

Wind direction distribution is shown in the wind rose histograms of Figure 5. These illustrations show, by means of a polar histogram, the dominant directions categorised by wind speed magnitude.

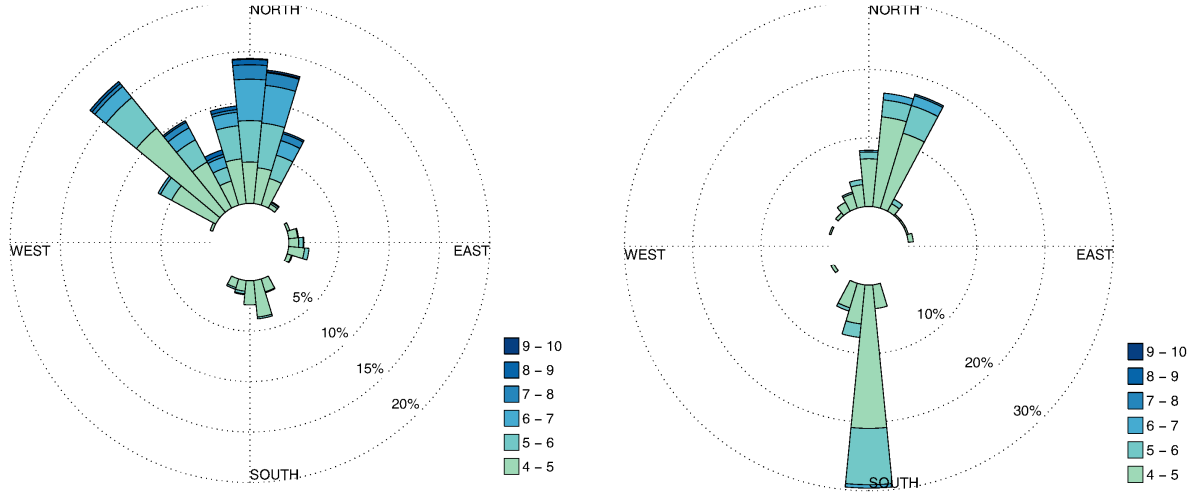

(a) (b)

Figure 5: Wind rose histograms of 10-min mean speed and corresponding direction for sonic anemometers: (a) WS1 and (b) WS2.

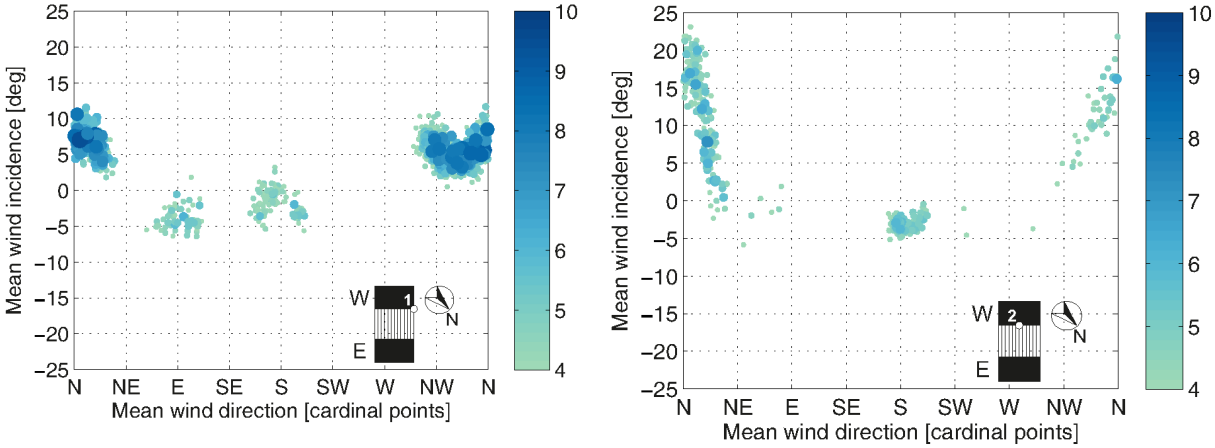

(a) (b)

Figure 6: Distribution of 10-min mean wind speed with direction and incidence angles measured by sonic anemometers: (a) WS1 and (b) WS2.

Besides the horizontal direction, Figure 6 depicts the distribution of the incidence angle and respective wind speed with the orientation. The negative and positive values of incidence account for descending and ascending angles respectively, while the size and shade of each point evidence the measured mean speed.

The presented results are in agreement with the expected wind behaviour for the structure's implantation in the terrain and the sensors position on the structure. As previously seen, the stadium is positioned approximately along the north-east – north-west axis (see Figure 1(a)) and the anemometers located on the west roof slab (see Figure 3). In both cases, the wind measured from south comes from the top of the west slab, accordingly it must have descending incidence angle, while the wind from the north-west - north-east sector flows from the stadium open side, reaching the anemometers with ascending incidence. The most unusual

results observed were the high incidence angles measured by the sonic anemometer WS2 (Figure 6(b)). These observations can be explained by the north and north-west winds that reach this sensor (located in the middle of the west slab as seen in Figure 3) being strongly influenced by the stadium structure.

4.2 Turbulence intensity

The turbulence intensity describes the characteristics of the fluctuating wind speed. The longitudinal, *u*, lateral, *v*, and vertical, *w*, turbulence intensities can be determined by the following equations:

$$I_u = \frac{\sigma_u}{\overline{U}}, \quad I_v = \frac{\sigma_v}{\overline{U}}, \quad I_w = \frac{\sigma_w}{\overline{U}} \tag{1}$$

where σ_u, σ_v and σ_w are the standard deviation or the RMS value of each fluctuating velocity component and $\overline{U}$ is the wind mean speed for the same time period. In this study, the same 10-minute period used before was adopted for the calculation of these parameters.

Figure 7 shows the variations of the longitudinal, lateral and vertical turbulence intensities as a function of the mean wind speed, independent of direction and incidence angles, for the anemometers WS1 and WS2. A general trend for $I_u > I_v > I_w$ is noticed across both sensors data.

The turbulence intensity is simply related to the surface roughness [11], and therefore to the wind incoming direction. In Figure 8 turbulence intensities from all incoming directions are represented, leading to a widespread distribution, especially in the case of WS2. Shown in Figure 8 are longitudinal, lateral and vertical turbulence intensities as a function of the 10-min mean wind direction, and the respective mean wind speed. From these, characteristic turbulence intensities can be identified by direction and a consistent evolution through direction is perceived.

Figure 9 shows the variation of the averaged longitudinal, lateral and vertical turbulence intensities as a function of the 10-min mean wind direction, categorised in sixteen 22.5º directional sectors. It is noted from Figure 9(a), corresponding to sensor WS1, that the three component turbulent intensities are rather homogeneous across all directions, with the exception of the two upward trends: one between SE and SSW; and other between N and WNW. On the other hand, measurements from wind sensor WS2 (see Figure(b)) reveal two rather distinct clusters: one, centred on the south direction, with an upward trend from SSE to SSW and a very narrow spread in direction; and another, centred on the north direction, with turbulence intensities generally greater than the first.

The variation of the averaged turbulence intensity ratios σ_v/σ_u and σ_w/σ_u as a function of mean direction, categorised in 16 directional sectors, is translated by Figure 10. Overlaid is the number of data points measured for each direction sector, expressed by a histogram.

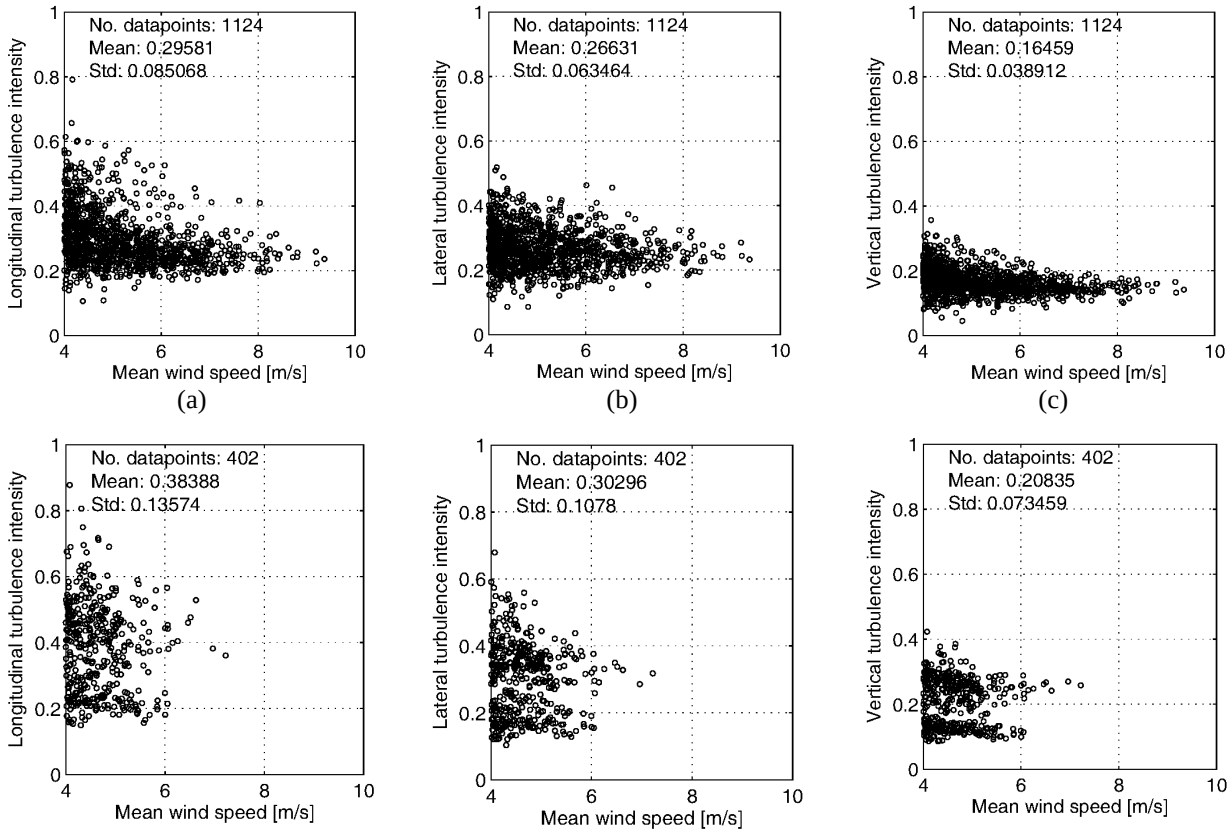

Figure 7: Variation of the turbulence intensity with the mean wind speed: (a) WS1 Longitudinal I_u; (b) WS1 Lateral I_v; (c) WS1 Vertical I_w; (d) WS2 Longitudinal I_u; (e) WS2 Lateral I_v; and (f) WS2 Vertical I_w.

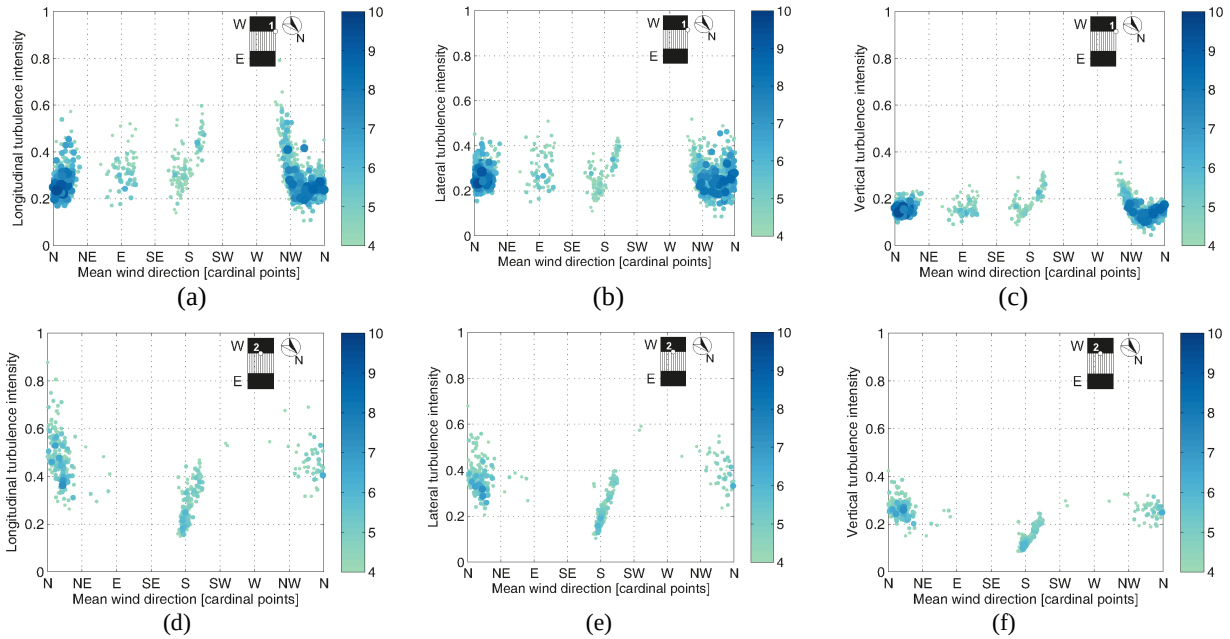

Figure 8: Variation of the turbulence intensity with the mean wind direction: (a) WS1 Longitudinal I_u; (b) WS1 Lateral I_v; (c) WS1 Vertical I_w; (d) WS2 Longitudinal I_u; (e) WS2 Lateral I_v; and (f) WS2 Vertical I_w.

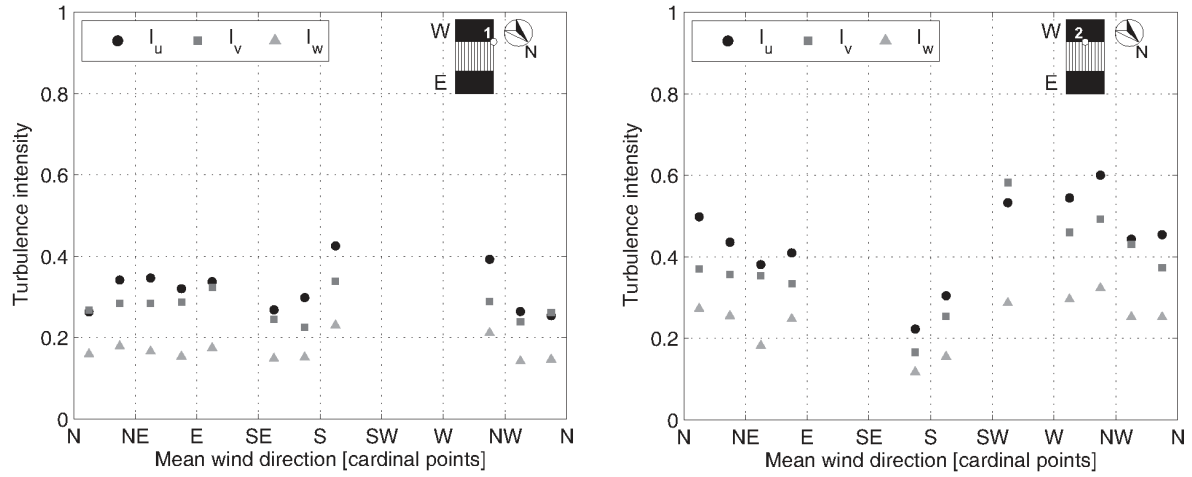

(a) (b)

Figure 9: Variation of averaged longitudinal, lateral and vertical turbulence intensities with 10-min mean wind direction measured by sonic anemometers: (a) WS1 and (b) WS2.

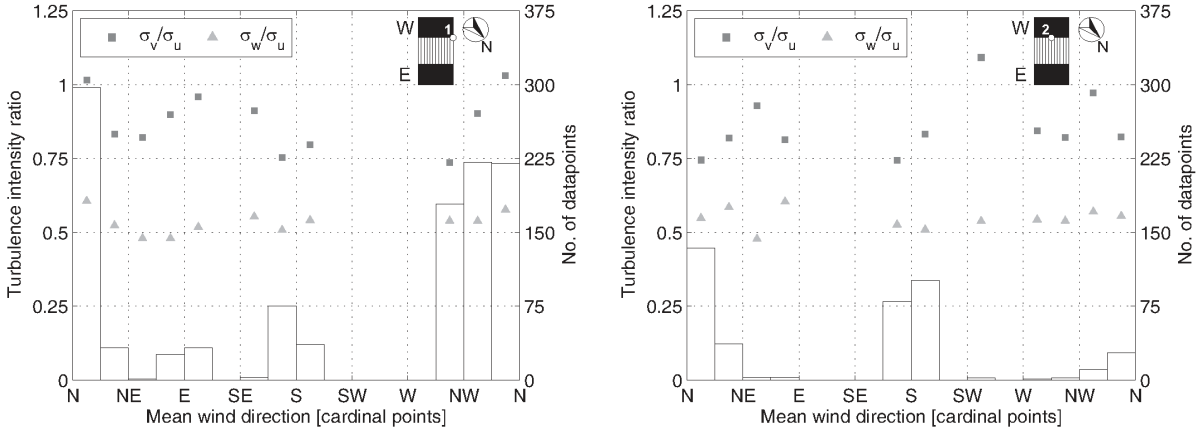

(a) (b)

Figure 10: Variation of averaged turbulence intensities ratios σ_v/σ_u and σ_w/σ_u as a function of 10-min mean wind direction: (a) WS1 and (b) WS2.

4.3 Power spectra of wind speed

Two samples of wind data with very distinct characteristics were selected for spectral analysis, both measured by sonic anemometer WS1. The criterion for this selection was the extraction of two-hour records with relatively high mean wind speed, but with opposite mean direction and incidence angles. Also, the wind sample should exhibit stationary characteristics, i.e., the mean wind speed from each segment should not differ more than 25 % from the wind speed mean of the full time series and, additionally, the corresponding direction angle must not vary by more than 15 deg [12].

The first sample chosen, with a north direction (15.9 deg) and an upward incidence (6.85 deg) was collected on 8 February 2012 between 11:50 and 13:50, and shows a mean wind speed of 7.73 m/s. The second sample, measured on the 25 April 2012 between 13:30 and 15:30, is characterised by a south direction (193 deg), a downward incidence (-2.94 deg) and a mean wind speed of 4.69 m/s.

The reduced auto power spectra computed for both wind samples for each turbulent component are depicted in Figure 11.

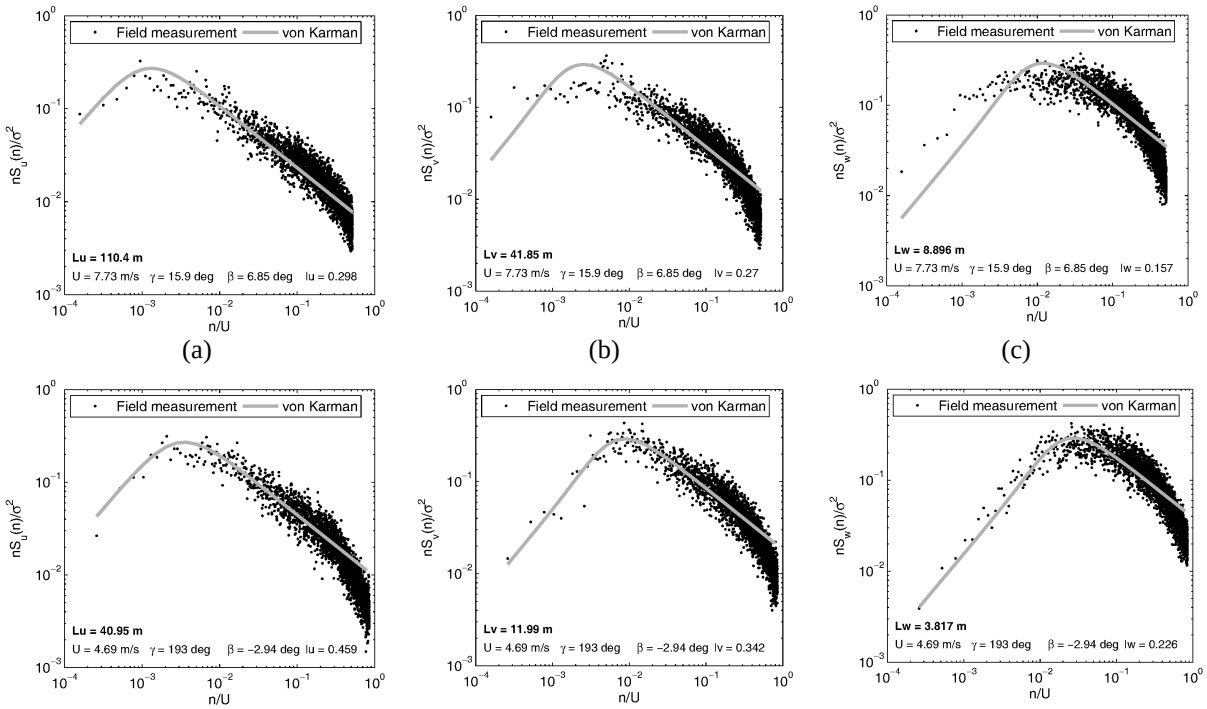

Figure 11: Power spectral density of wind measured by ultrasonic anemometer WS1. north – 8/2/2012: (a) along-wind; (b) cross-wind; (c) vertical wind; south – 25/4/2012 (d) along-wind ; (e) cross-wind; (f) vertical wind.

4.4 Turbulence integral length scales

The turbulence length scales define the average size of the turbulent eddies of the flow. The von Kármán spectra fitted to the power spectra density functions are represented in Figure 11, together with the resulting integral length scale. The values of the turbulence integral length scale obtained for the along-wind, cross-wind and vertical wind directions are, respectively, 110.4 m, 41.85 m and 8.896 m for northern winds and 40.45 m, 11.99 m and 3.817 m for southern winds. A prominent distinction is found between the parameters obtained for the two opposite prevailing directions. Turbulence integral length scales from northern winds present values 2-3.5 times greater than those measured from southern winds.

5 MODAL PARAMETERS

The automatic identification of the modal parameters (natural frequencies, mode shapes and damping ratios) is performed based on the ambient vibration response continuously measured by the dynamic monitoring system. For this purpose, developed algorithms process 60-minute acceleration files using the Covariance driven Stochastic Subspace Identification method (SSI-COV) complemented with a methodology based on the hierarchical clustering algorithm to automatically interpret stabilisation diagrams [13].

Table 1 summarises the mean and standard deviation values obtained for the analysis of the natural frequencies and damping ratios identified between December 2011 and August 2012. Representation of the corresponding modal configurations is shown in Figure 12.

Mode	Frequency [Hz]		Damping [%]	
	mean	std	mean	std
1	0.275	0.001	0.21	0.12
2	0.290	0.001	0.19	0.11
3	0.526	0.002	0.21	0.08
4	0.542	0.001	0.17	0.07
5	0.555	0.004	0.38	0.13
6	0.631	0.002	0.27	0.09
7	0.653	0.001	0.21	0.06
8	0.680	0.004	0.15	0.06
9	0.696	0.002	0.14	0.05
10	0.731	0.003	0.14	0.06
11	0.862	0.004	0.33	0.12
12	1.002	0.005	0.40	0.10

Table1: Mean and standard deviation values of the natural frequencies and damping ratios identified in the period between December 2011 and August 2012.

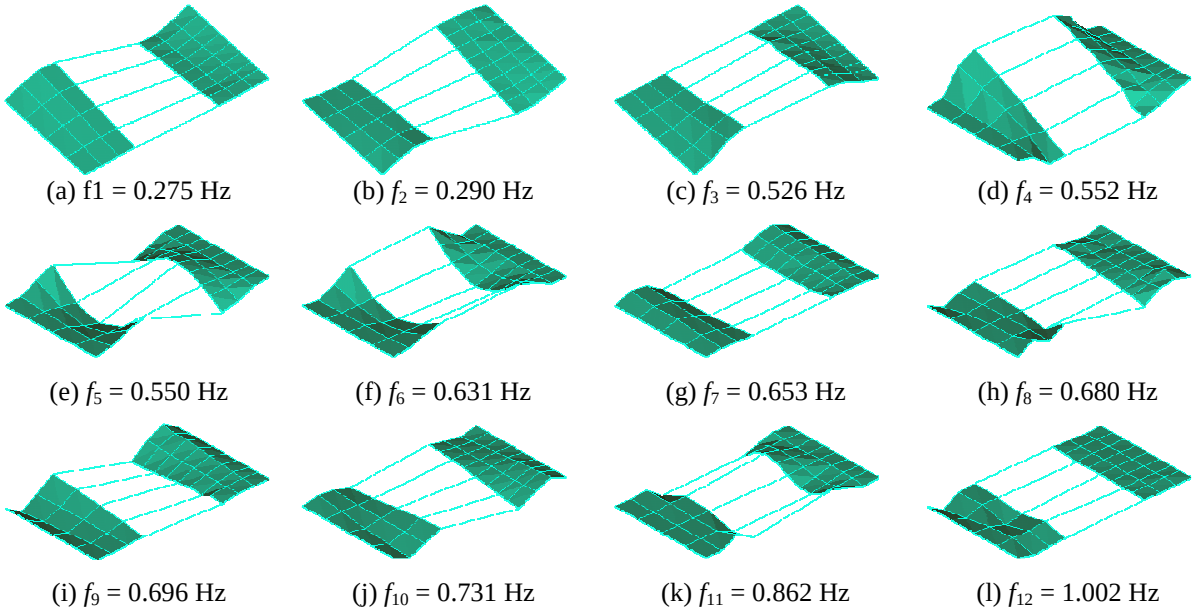

(a) f1 = 0.275 Hz (b) f_2 = 0.290 Hz (c) f_3 = 0.526 Hz (d) f_4 = 0.552 Hz

(e) f_5 = 0.550 Hz (f) f_6 = 0.631 Hz (g) f_7 = 0.653 Hz (h) f_8 = 0.680 Hz

(i) f_9 = 0.696 Hz (j) f_{10} = 0.731 Hz (k) f_{11} = 0.862 Hz (l) f_{12} = 1.002 Hz

Figure 12: Identified modal configurations associated with the first twelve modes [3].

6 INFLUENCE OF WIND ON THE STRUCTURAL RESPONSE

In this section, the influence of wind speed on structural response is described by the relationship between the 10-min root-mean-square (RMS) acceleration response and the mean wind speed and direction for the same period of time. The vertical acceleration response measured by the six accelerometers of the monitoring system was analysed for periods of time in which the 10-min mean wind speed measured by WS1 (Figure 3) were greater than 4 m/s. Furthermore, the analysis took into account the 10-min mean wind direction, dividing acceleration responses according to sixteen 22.5º directional sectors.

Figure 13 shows the relationship between the mean wind speed measured by WS1 and the vertical RMS accelerations measured by each accelerometer according to the three dominant

wind directions. From the performed analysis only the three directional sectors between 315º (NW) and 22.5º (NNE) showed a reasonable amount of observations.

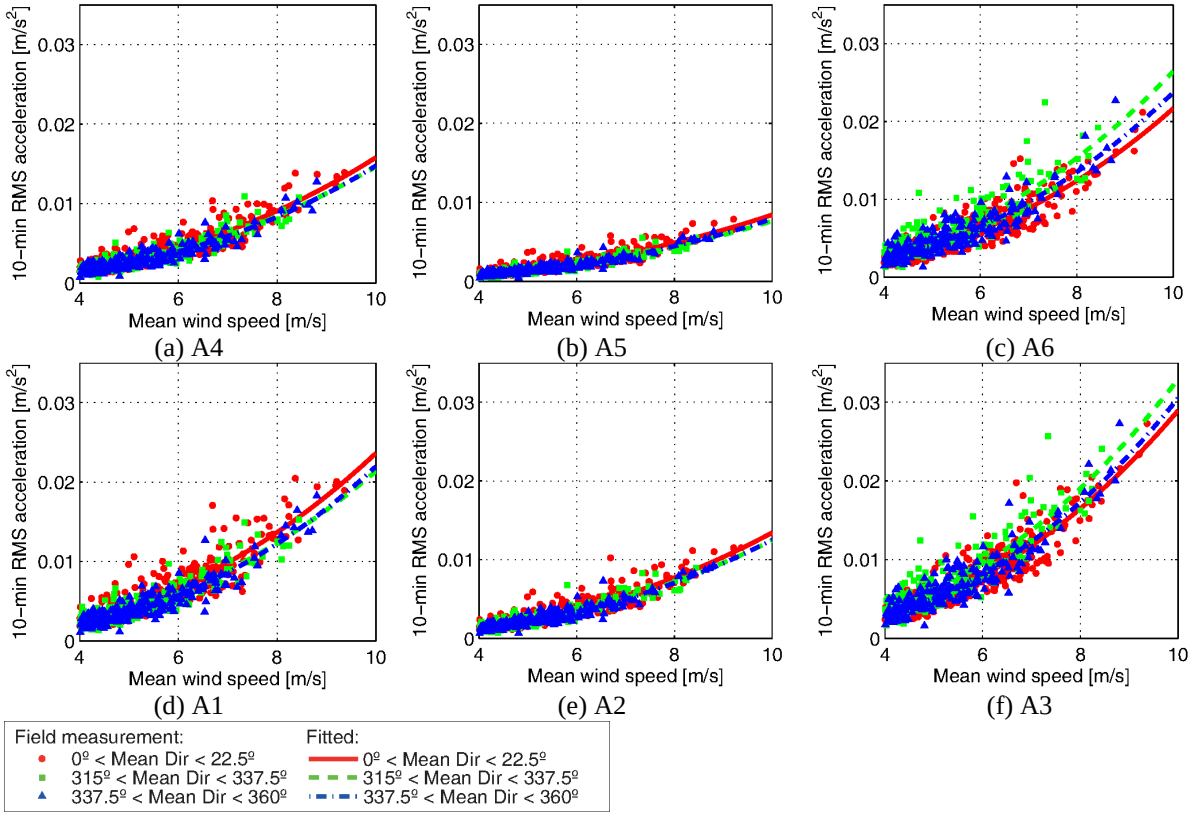

Figure 13: Relationship between mean wind speed from 3 dominant wind directions and 10-min RMS acceleration (see Figure 3).

The analysis of Figure 13 clearly shows the similarities in acceleration magnitude between accelerometers in the same suspension roof longitudinal direction (A1-A4, A2-A5 and A3-A6) (see Figure). It is also noticeable that sensors placed near the slab inner edge (A1, A2 and A3) show higher RMS accelerations than the corresponding sensors placed along the middle of the slab (A4, A5 and A6). The acceleration levels observed for each of the six accelerometers, and the relation between them, reflect the modal shapes of the first vibration modes (see Figure 12). The accelerometers placed on the north-west border of the slab (A3 and A6) show the highest magnitudes of acceleration, with nearly 0.03 m/s^2 RMS and 0.13 m/s^2 maximum for the higher wind speeds.

7 INFLUENCE OF WIND SPEED AND TEMPERATURE ON THE NATURAL FREQUENCIES AND MODAL DAMPING RATIOS

The modal parameters identified by the dynamic monitoring system reflect the influence of environmental and operational factors. In order to analyse the dependence between the mean wind speed, the ambient temperature variation and the value of the identified natural frequencies, the Pearson correlation coefficients were computed. Table 2 summarises the measures of correlation found between the identified natural frequencies and the mean wind speed and temperature.

	Natural frequency of mode:											
	1	2	3	4	5	6	7	8	9	10	11	12
$\overline{U}$	-0.28	-0.27	0.03	0.08	-0.26	-0.34	-0.37	-0.30	-0.21	-0.18	-0.46	-0.38
$\overline{T}$	-0.60	-0.69	0.76	0.62	-0.36	-0.04	-0.44	-0.59	-0.66	-0.61	-0.41	-0.34

Table 2: Pearson correlation coefficients between the natural frequency values and the mean wind speed and mean sonic temperature.

It is evident from the analysis of Table 2 that, apart from modes 3 and 4, the value of natural frequencies tends to vary inversely with both the mean wind speed and the mean temperature. The correlation with the mean wind speed in modes 3 (Figure 14(a,d)) and 4 is the smallest observed, with values close to zero, and contrary to the general trend, the value of the natural frequency tends to increase with higher ambient temperatures. An overall trend for a greater correlation between the natural frequencies and the mean temperature than with the mean wind speed is observed across Table 3. Exceptions are found for mode 6 (Figure 14 (b,e)), where the correlation with mean temperature is approximately zero, and modes 11 (Figure 14(c,f)) and 12, that show a similar degree of correlation with both variables.

To further investigate the effect of mean wind speed and mean temperature variation on the value of natural frequencies, the following linear regression was applied:

$$f_i = \beta_0 \overline{T} + \beta_1 \overline{U} + \beta_2 \tag{2}$$

where f_i is the natural frequency, $\overline{T}$ is the mean temperature, $\overline{U}$ is the mean wind speed, and β_0, β_1 and β_2 are fitting parameters.
Table 3 lists the regression parameters and the R^2 value for each mode.

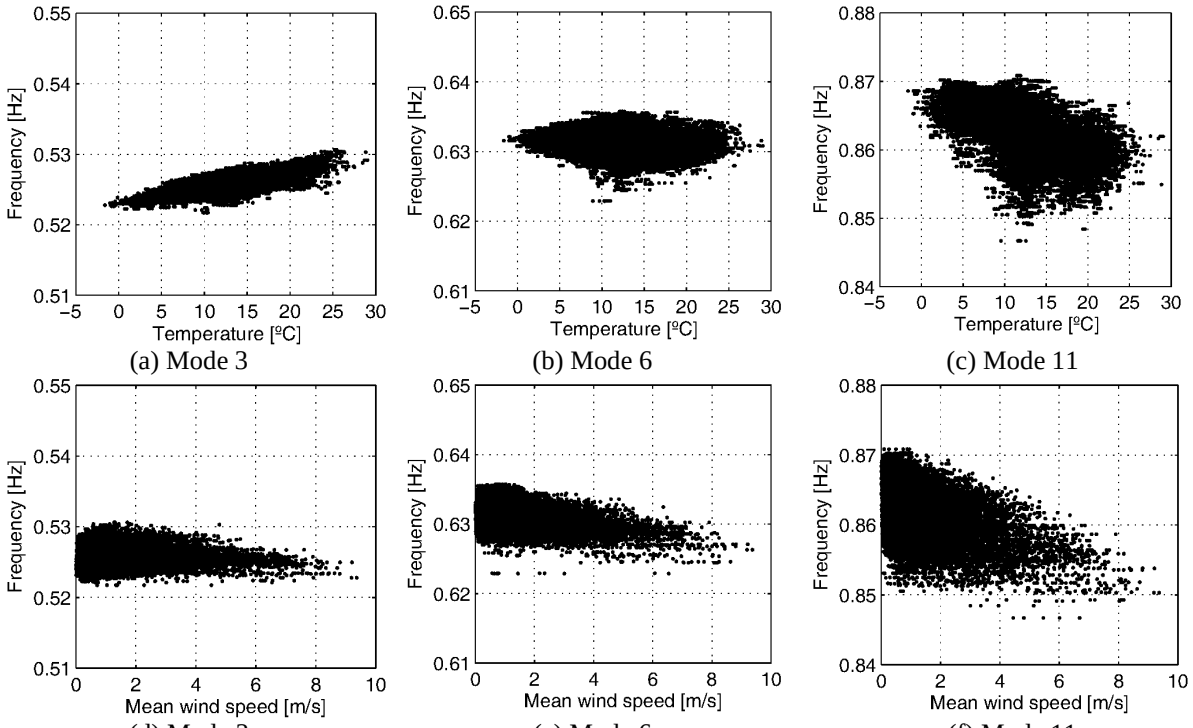

Figure 14: Correlation between the identified natural frequencies and: (a,b,c) mean sonic temperature; and (c,d,e) mean wind speed; for modes 3, 6 and 11.

Mode	β_0 [x10^{-4} Hz $^oC^{-1}$]	β_1 [x10^{-4} Hz (m/s)$^{-1}$]	β_2 [Hz]	R^2
1	-0.65	-0.99	0.275	0.53
2	-1.19	-1.47	0.292	0.64
3	2.08	-0.49	0.523	0.58
4	1.35	0.46	0.540	0.30
5	-2.51	-7.00	0.554	0.19
6	-0.53	-4.46	0.632	0.14
7	-0.93	-3.38	0.654	0.35
8	-2.17	-5.29	0.683	0.14
9	-2.48	-1.87	0.699	0.48
10	-3.54	-2.23	0.736	0.35
11	-3.62	-13.25	0.868	0.45
12	-2.71	-17.12	1.007	0.29

Table 3: Regression parameters between the identified natural frequencies, the mean sonic temperature and the mean wind speed measured by WS1.

It is worth noting that the natural frequencies of modes 10 and 11 show a greater sensibility to temperature change, while values from modes 1 and 6 are the least sensitive to this variable. Frequencies from modes 11 and 12 show higher variations with mean wind speed change. On the other hand, values corresponding to modes 3 and 4 show the smallest influence.

To study the relationship between damping ratios and the mean temperature and mean wind speed, the Pearson correlation coefficients between these variables were calculated. Table 4 summarises the most important results of the correlation analysis. The analysis of this table shows a trend for the identified damping ratios to vary proportionally with both the mean wind speed and the mean temperature, the only exception being the almost null correlation coefficient with temperature of the damping ratio associated with mode 11. The main conclusion is that for all investigated modes the variation of the damping ratio is more associated with the change of mean wind speed than of mean temperature. For this reason, only the relationship between damping ratios and mean wind speed has been considered in subsequent analyses.

	Damping ratio of mode:											
	1	2	3	4	5	6	7	8	9	10	11	12
$\bar{U}$	0.49	0.48	0.46	0.41	0.34	0.36	0.40	0.50	0.37	0.43	0.35	0.46
$\bar{T}$	0.17	0.18	0.17	0.13	0.27	0.19	0.13	0.18	0.14	0.21	-0.05	0.27

Table 4: Pearson correlation coefficients between identified damping ratios and the mean wind speed and mean sonic temperature.

Figure 15 represents the relation with mean wind speed of the identified damping ratios for modes 1, 3 and 9. The approximately linear relationship observed in the range of measured mean wind speed is common to all identified modes and reflects the wind induced added damping to the total identified damping ratio.

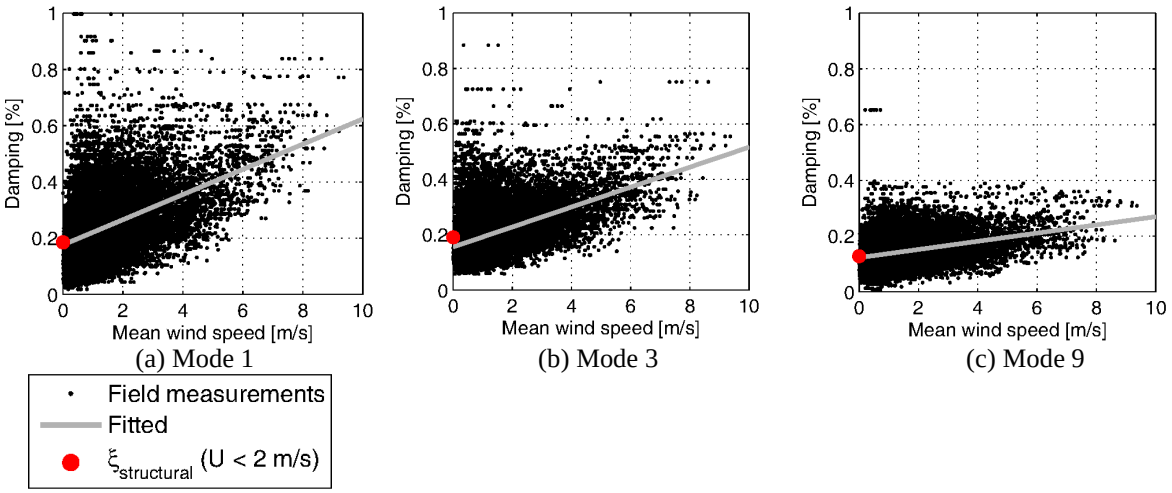

Figure 15: Correlation between the identified damping ratio and the mean wind speed; for modes (a) 1, (b) 3 and (c) 9, including the least-square fit and structural damping computed from low wind speeds.

The damping measurements corresponding to periods of very low wind speeds (lower than 2 m/s) were averaged for each mode in order to obtain an estimate of the structural damping ($\xi_{structural}$). In a different approach, least-squares linear fit was applied to the identified damping points associated with mean wind speed higher than 2 m/s. The constant term of the fitted line provides alternatively an estimate of the structural damping, while the slope parameter expresses the wind induced added damping gradient ($\Delta\xi_{aerodynamic}$) [14].

A great resemblance for the estimated structural damping values is found across all modes, with a general trend for greater values obtained by the averaging approach at low wind speed. The computed values for wind induced added damping range from 0.015 % $(m/s)^{-1}$, for mode 9, to 0.060 % $(m/s)^{-1}$, for mode 11, and correspond to an average of 20 % of the structural damping per m/s. The quality of the least-square linear fits is generally low, due to the significant scatter of the identified damping ratios.

8 CONCLUSIONS

Combining recent developments in terms of sensors, data communicating systems, computational power and identification algorithms, the continuous monitoring program established around the suspension roof of the Braga stadium has allowed the continuous measurement of wind, temperature and acceleration. The variation of such quantities during a period of 8 months has been investigated, with the purpose of obtaining a characterisation of the wind action based on field tests, establishing correlations with the structural response and finally analysing the influence of wind and temperature on the variation of modal parameters.

The measurement of wind using two sonic anemometers mounted on one of the slabs has permitted the identification of dominant directions, incidences and intensity of the typical wind speed, as well as allowed the characterisation of the intensity of turbulence and the spectral content, for the purpose of future verification of the design wind model.

The measurement of acceleration at 6 points along one of the slabs has allowed the establishment of response correlations with the wind velocity, which will be used as well to verify corresponding information obtained from wind tunnel tests at design stage.

Finally, the continuous identification of modal parameters together with wind and temperature measurements have allowed the investigation of the latter parameters on their variation.

Despite the low wind velocity generally measured and considering the corresponding interval of variation, it has been shown that most natural frequencies are simultaneously influ-

enced by temperature and wind, although temperature generally plays a dominant role, even if having a varying importance according to the vibration mode.

As for damping ratios, whose estimates typically exhibit higher scatter, and again despite the low wind velocity, it was possible to evidence the dominant influence of wind and, using two different approaches, separate the structural from the aerodynamic damping components, with very satisfying agreement, also confirmed by previous estimates based on free and forced vibration methods.

ACKOWLEDGEMENTS

The authors would like to acknowledge: (1) all the supports provided by the Portuguese Foundation for Science and Technology (FCT) to ViBest / FEUP, particularly in the context of Projects "Wind analysis of special structures from full scale measurements" and "DYNAMO_DEMO - Advanced Tools for Dynamic Structural Health Monitoring of Bridges and Special Structures" (2) the support of AFA Consult (Engº Carlos Quinaz) and Câmara Municipal de Braga; (3) the Ph.D. Scholarship (SFRH/BD/44291/2008) provided by FCT to the third author.

REFERENCES

[1] R. Furtado, C. Quinaz, R. Bastos, "New Braga Municipal Stadium, Braga," *Structural Engineering International*, vol. 2, pp. 72–76, 2005.

[2] E. Caetano, "Numerical modeling of the structural behaviour of the new Braga Stadium roof," Porto, Portugal, Technical Report, 2001.

[3] E. Caetano, Á. Cunha, F. Magalhães, "Numerical and experimental studies of the Braga Sports Stadium suspended roof," *Structure and Infrastructure Engineering*, vol. 6, no. 6, 2010, pp. 715–724.

[4] F. Magalhães, E. Caetano, Á. Cunha, "Operational modal analysis and finite element model correlation of the Braga Stadium suspended roof," *Engineering Structures*, vol. 30, no. 6, 2008, pp. 1688–1698.

[5] M. Majowiecki, N. Cosentino, "Dynamic aspects of the New Braga Stadium large span roof," *Proceedings of IASS Symposium*, 2007.

[6] F. Magalhães, Á. Cunha, E. Caetano, "Installation of a Continuous Dynamic Monitoring system at Braga Stadium Suspended Roof: initial results from automated modal analysis," in *EVACES 2009, Wroclaw, Poland*, 2009.

[7] N. Martins, A. Cardoso, E. Caetano, "Development of an observation system based on anemometry to characterize the wind action over a suspension roof," in *YIC2012*, 2012.

[8] F. Magalhães, E. Caetano, Á. Cunha, "Operational modal analysis of the Braga sports stadium suspended roof," in *IMAC XXIV, St. Louis, MO*, 2006.

[9] J. C. Kaimal, J. J. Finnigan, *Atmospheric boundary layer flows: their structure and measurement*. Oxford University Press, USA, 1994.

[10] J. M. Wilczak, S. P. Oncley, S. A. Stage, "Sonic anemometer tilt correction algorithms," *Boundary-Layer Meteorology*, vol. 99, no. 1, 2001, pp. 127–150.

[11] J.D. Holmes, "*Wind Loading of Structures*", Spon Press, 2001.

[12] C. Cremona, J.-C. Foucriat, "*Comportement au Vent des Ponts*", Presses de l'École Nationale des Ponts et Chaussées, 2002.

[13] F. Magalhães, Á. Cunha, E. Caetano, "Online automatic identification of the modal parameters of a long span arch bridge," *Mechanical Systems and Signal Processing*, vol. 23, no. 2, 2009, pp. 316–329.

[14] J. H. G. Macdonald, "Separation of the contributions of aerodynamic and structural damping in vibrations of inclined cables," *Journal of Wind Engineering and Industrial Aerodynamics*, vol. 90, no. 1, 2002, pp. 19–39.